Materials Science Forum
ISSN: 1662-9752, Vol. 1186, pp 1-11
doi:10.4028/p-wwLq8G

Submitted: 2026-01-15
Revised: 2026-02-27
Accepted: 2026-02-27
Online: 2026-04-16

Experimental-Numerical Approach to Determine the Heat Transfer Coefficients for Compound Forging Processes

Mohnfeld Norman[1,a*], Schute Marie[1,b], Peddinghaus Simon[1,c], Uhe Johanna[1,d] and Behrens Bernd-Arno[1,e]

[1]Leibniz University Hannover, Institute of Forming Technology and Machines (IFUM), An der Universität 2, 30823 Garbsen, Germany

[a*]mohnfeld@ifum.uni-hannover.de, [b]marie.schute@stud.uni-hannover.de, [c]s.peddinghaus@ifum.uni-hannover.de, [d]uhe@ifum.uni-hannover.de, [e]behrens@ifum.uni-hannover.de

[*]corresponding author

Keywords: heat transfer coefficient, compound forging, experimental-numerical approach.

Abstract. For the reliable numerical simulation and design of compound forging processes involving dissimilar materials, an accurate representation of thermal boundary conditions is essential. In particular, the heat transfer coefficient (HTC) at the interface of the workpiece and the die strongly influences temperature distribution, material flow, and interfacial integrity. Despite its significance, the HTC is frequently modelled as constant in finite element (FE) simulation due to the lack of experimental data for forging-relevant conditions. Therefore, this study presents an experimental–numerical methodology for determining load-dependent HTCs representative of compound forging. A specialised test setup was used to reproduce the thermal–mechanical boundary conditions of hot bulk forming, by inducing contact pressures both below and above the flow stress of the workpiece material. Temperature histories were recorded using embedded thermocouples and analysed through an inverse numerical approach based on a one-dimensional (1D) finite element (FE) model. The influence of contact pressure, heating atmosphere, and lubrication on the HTC was systematically investigated for a S235JR specimen temperature of 600 °C. The results demonstrate a pronounced pressure dependency of the HTC, with increasing values at higher contact pressures. Oxide formation and lubrication were shown to significantly affect heat transfer behaviour, particularly while heating under atmospheric conditions. The presented approach provides process-specific HTC data that can substantially improve the predictive capability of numerical simulations for compound forging applications.

Introduction

The reduction of vehicle weight is a key strategy within the automotive sector to lower CO_2 emissions. While highly developed lightweight solutions have been established in sheet metal forming, their transfer to bulk metal forming remains comparatively limited [1]. As the total mass of bulk-formed components in vehicles is approximately equivalent to that of sheet metal parts, substantial lightweight potential exists in this domain [2]. Hybrid components made from at least two different materials offer great potential as a new technology for innovative lightweight construction concepts. Using hybrid components allows the advantageous properties of each material to be exploited in a targeted manner, thereby reducing component weight while maintaining the same load capacity. Compound forging enables load-adapted component structures by joining distinct materials within a single forming operation. This facilitates resource-efficient highly productive fabrication of near-net-shape hybrid components. During forming, the dissimilar materials are bonded through a combination of mechanical interlocking and metallurgical joining. The process chain consists of the pre-joining of semi-finished parts by form or force fit, followed by targeted inhomogeneous inductive heating to establish material-specific temperatures, and compound forging to a hybrid component [3].
Hybrid components made of aluminium and steel offer an excellent combination of weight reduction through the aluminium on the one hand and increased strength through the steel on the other. The

joining of dissimilar materials such as steel and aluminium presents significant challenges, primarily due to the different forming temperatures and the formation of intermetallic phases (IMP). The thermal conditions at the material interfaces critically influence the forming behaviour and the IMP formation. Heat transfer from the hotter steel to the aluminium may locally exceed the aluminium solidus temperature, causing partial melting and impairing the bond. Also, heat loss of the steel billet may reduce its formability and increase the risk of damage failure. Additionally, continuous heat transfer occurs from the billets to the colder die surfaces [3, 4]. Accurate description of the temperature distribution within the semi-finished parts and tools is therefore essential for a precise process design and simulation. Finite element modelling has proven capable of fulfilling this purpose; however, its accuracy strongly depends on the correct representation of process-specific thermal boundary conditions [5].

A key parameter in modelling thermal interactions is the HTC α at the workpiece–die interface, which depends on time-varying process quantities such as contact pressure (σ_N), surface temperatures ($T_{\mathrm{workpiece}}$, T_{die}), and lubrication conditions ($n_{lubrication}$) [5,6]. Despite its relevance, the HTC is commonly treated as a constant in numerical simulations due to insufficient experimental data [7], thereby limiting predictive accuracy. The experimental characterisation of the HTC is extremely challenging due to the difficult accessibility of the contact area and the control of the test parameters. Experimental determination of the HTC requires temperature measurements near or at the contact interface. Direct approaches, such as tool-surface thermocouples, often interfere with the contact and compromise the measurement, while thermography is not applicable in closed-die conditions [5]. Indirect methods, whereby thermocouples are embedded close to the die surface, are thus commonly employed. By reproducing experimental conditions numerically and iteratively matching the simulated temperature histories to the measured, the HTC can be determined. Fundamental studies using such indirect approaches were presented by Singh et al. [8], Dixit et al. [9], and Volke et al. [10]. Additional contributions include Wen et al. inverse heat conduction analysis for warm sheet forming [6] and Bhattacharya et al.'s characterisation of HTC during press hardening, highlighting the contact pressure as the dominant influence factor [11].

Most of these investigations rely on a test rig developed by Volke et al., involving two heated opposing punches with integrated temperature sensors [10]. However, generating homogeneous initial temperature fields and controlling relevant parameters, such as contact pressure or position of the thermocouples is experimentally demanding. Furthermore, existing studies predominantly address sheet metal forming, whereas bulk forming involves substantially higher contact pressures and a greater thermal mass, leading to slower cooling rates and increased thermal inertia of the workpiece. In processes such as compound forging in closed dies, contact pressures may exceed the material flow stress due to superimposed hydrostatic pressure states.

To this day, no detailed investigation of the HTC under the specific thermal–mechanical conditions of compound forging has been reported. This study presents an extension of the experimental setup by Mohnfeld et al. [12] for recording the HTC of steel for composite forging. In order to prevent the aluminium from melting due to the steel during heating, the HTC was investigated for a steel temperature of 600 °C under varying process boundary conditions. The approach enables the coupled experimental–numerical determination of a load-dependent HTC, providing essential data for accurate modelling and process design.

Methods - Experimental Investigation

The system was mounted in a servo-hydraulic forming simulator (Instron), as shown in Fig. 1. The test set-up consists of three steel plates guided laterally by two columns. The upper plate is fixed to a strain gauge-based load cell (Kistler) and rigidly guided by the outer columns. The columns are fixed against the lower frame of the forming simulator using adjustable feet. The centre plate is mounted in a floating configuration via springs. A U-shaped cavity in the centre plate bears the specimen holder and ensures its alignment between the punches. The lower plate is connected to the hydraulic cylinder. When the cylinder moves towards the force load cell, the springs are compressed, thereby continuously centring the middle plate between the upper and lower plates. This ensures a

simultaneous contact of the upper and lower punches to the specimen. To protect the system from the temperatures typical for hot bulk forming of up to 1,100 °C, cooling channels were added into the plates and connected via hoses, as shown in Fig. 1(a). A continuous water flow through these channels enables a rapid heat extraction from the specimen holder, thereby maintaining reproducible testing conditions and shielding the bearings and columns from thermal loads. The functional principle of the specimen holder (1.2343), the specimen (S235 JR), and the punches (1.2343) is shown schematically in cross-section in Fig. 1(b). The tool steel 1.2343 was chosen because the dies are made from 1.2343 in the subsequent compound forging process, and S235JR is a workpiece material used in the compound forging process. The steel specimen is fixed in the specimen holder, which can be closed in a form-fit manner by rotating the locking mechanism around the z-axis. Openings in both the specimen holder and the lock allow the punches to contact the specimen's end faces. Once the punches establish contact, the specimen is fully enclosed, generating a hydrostatic stress state. This enables the investigation of contact stresses exceeding the flow stress of the specimen material. Each punch has a drilled hole into which a type-K thermocouple (TC1, TC3) is inserted to within 0.9 mm of the punch face, allowing near-surface measurement of the punch temperature during contact heating. An additional thermocouple (TC2) positioned via a lateral bore in the specimen holder measures temperature directly at the specimen surface. Two thermocouples were placed between U-shaped cavity and the cooling channel in the central plate to record its thermal evolution.

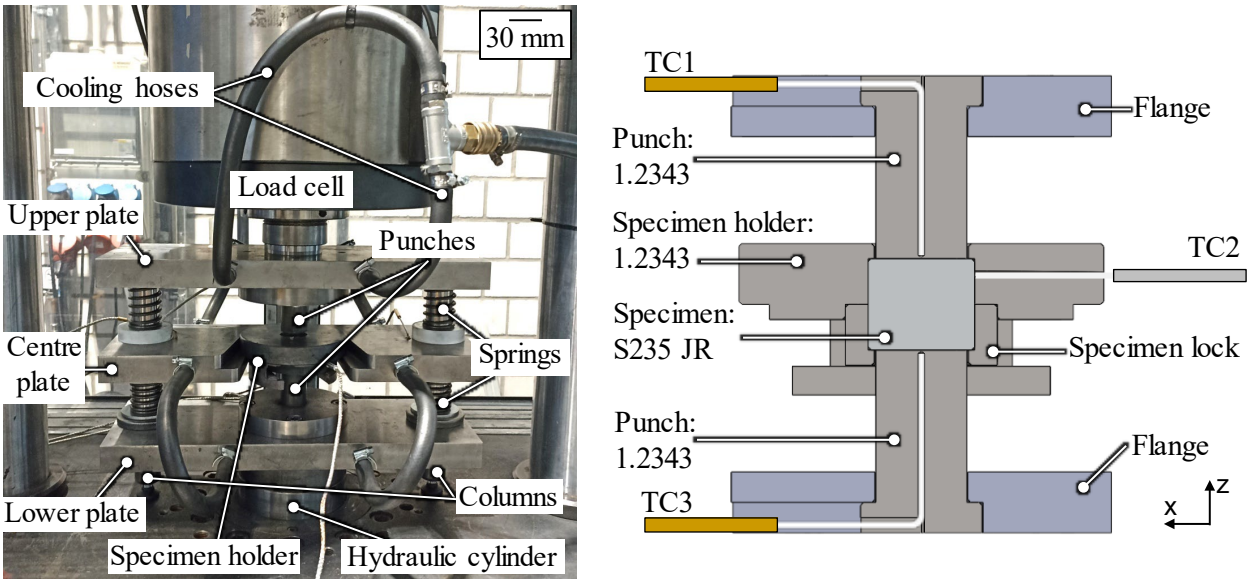

(a) (b)

Fig. 1. (a) Test set-up for determining the HTC under forging-relevant process parameters according to Mohnfeld et al. with extended cooling system, (b) Schematic cross-sectional view of the active components of the experimental setup [12].

Prior to testing, the specimen holder is equipped with the specimen and heated to the test temperature in a chamber furnace (Nabertherm). The specimen temperature is monitored via the thermocouple in the specimen holder. The transfer time from furnace to test rig remained below 20 s, following the requirement defined in [12]. A combined loading profile was used to ensure a rapid punch–specimen contact and thereby avoid premature cooling of the specimen surface. First, a position-controlled pre-alignment is carried out; then switches to a load-controlled motion until the target force is reached upon specimen contact. The target force is maintained for 60 s, and then removed. The investigated parameter combinations are listed in Table 1. All tests were performed at a specimen temperature of 600 °C in order to test the integrated cooling system of the test rig and to record the heat transfer for the composite forging of EN AW-6082 and S235JR for the maximum contact zone temperature. The pressure dependency of the HTC was examined using six contact pressures in the range of 50–550 MPa.

The flow stress from S235JR at 600 °C, at a quasi-static strain rate of 0.1 s^{-1} and a strain of 0.2, is around 300 MPa, meaning that three pressures below and three above the material's flow stress were investigated [13].

Table 1. Experimental matrix for determining a load-dependent HTC (fully factorial).

Temperature in °C	Load in MPa (kN)	Lubrication	Atmosphere	Repetitions
600	50 (35.34) 150 (106.03) 250 (176.71) 350 (247.40) 450 (318.09) 550 (388.77)	none ConTraer G300 LUBRODAL F 3670	Air Argon	3

To determine the influence of scale formation on the HTC, all parameter combinations were tested both with and without a protective gas atmosphere. Argon 5.0 was used as the protective gas, and the furnace was continuously flooded at a flow rate of 6.6 l/min. In hot bulk forming, lubricants are used not only to influence tribological conditions between die and workpiece but also the thermal interaction. The lubricants ConTraer G300 and LUBRODAL F 3670 (Fuchs Lubritech) were evaluated and applied to the punch faces prior to testing. ConTraer G300 was applied with a spray duration of approx. 4 s, whereas LUBRODAL F 3670 was applied using a soaked sponge following a pad-printing approach [14]. Before each test, the punches were cleaned and fresh lubricant was applied. Each parameter combination was repeated three times.

Methods - Numerical Investigation

The determination of HTC was carried out using an iterative inverse optimisation based on the experimentally recorded temperature histories. The developed MATLAB script consists of a one-dimensional finite element (1D FE) model and an optimisation module. The basis of the 1D FE model is the discretisation of the test setup, whereby the specimen and the punch are represented as discrete node chains. Heat conduction within the materials is modelled using Fourier's law Eq. 1, while the heat transfer between the two materials is described according to Newton's law of cooling, Eq. 2 [12]. Heat loss through heat radiation is described by the Stefan-Boltzmann law in Eq. 3.

$$\dot{Q}_{heat\ conduction} = \frac{A \cdot \lambda \cdot \Delta T}{s} \tag{1}$$

$$\dot{Q}_{heat\ transfer} = \alpha \cdot A \cdot \Delta T \tag{2}$$

$$\dot{Q}_{heat\ radiation} = \epsilon \cdot \sigma \cdot A_M \cdot \Delta T^4 \tag{3}$$

$$\dot{U} = \frac{\dot{Q}}{m \cdot c_p} \tag{4}$$

The nomenclature of the energy balances (Eq. 4) for heat conduction, heat transfer, and thermal radiation is illustrated in Fig. 2(a). Fig. 2(b) schematically shows the 1D FE model of the punch, the specimen, and the specimen holder.

Temperature	T_x
Stefan-Boltzmann-constant	σ
Thermal conductivity	λ_x
Specific heat capacity	$c_{p,x}$
Heat transfer coefficient	α
Mass	m_x
Step size	s
Surface	A_x
Emissivity	ϵ

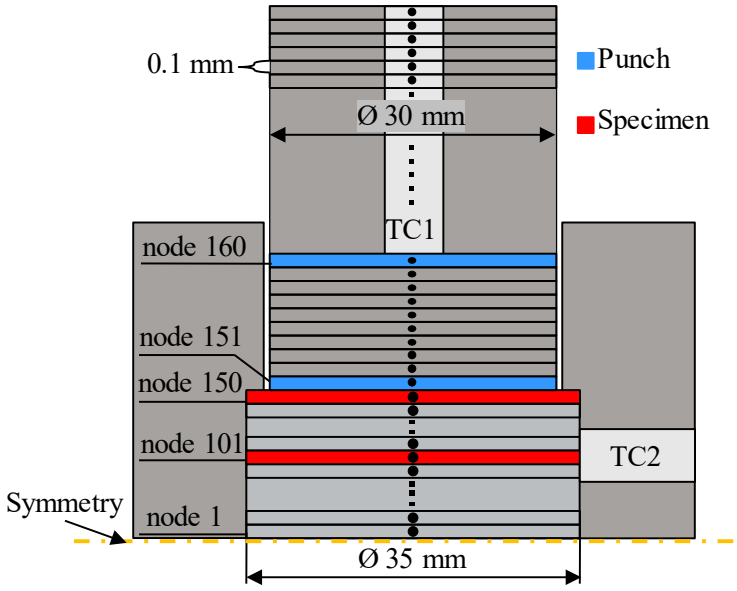

(a) (b)

Fig. 2. (a) Nomenclature of the fundamental equations, (b) Schematic representation of the 1D FE model.

To reduce computational effort, only one half is considered, with the plane of symmetry located at the centre of the specimen. The model consists of 500 nodes, where nodes 1–150 represent the specimen and nodes 151–500 correspond to the punch. The energy balance for the punch nodes including the heat radiation is shown in Eq. 5.

$$\dot{U}_x = \frac{A \cdot \lambda_{T,punch} \cdot (T_{x-1} - T_x)}{m_{punch} \cdot c_{p,T,punch} \cdot s} - \frac{A \cdot \lambda_{T,punch} \cdot (T_x - T_{x+1})}{m_{punch} \cdot c_{p,T,punch} \cdot s} - \frac{\epsilon \cdot \sigma \cdot A_M \cdot (T_x^4 - T_A^4)}{m_{punch} \cdot c_{p,T,punch}} \quad (5)$$

The experimental test temperature is initially assigned to the specimen nodes, while the punch nodes are assigned an initial temperature of 25 °C. As a boundary condition, the experimentally measured temperature history from the specimen holder is assigned to node 101. Nodes 150 and 151 represent the contact nodes, at which the HTC is incorporated into the energy balance, Eq. 6 for node 150.

$$\dot{U}_{150} = \frac{A_{specimen} \cdot \lambda_{specimen} \cdot (T_{149} - T_{150})}{m_{specimen} \cdot c_{p,specimen} \cdot s} - \frac{\alpha \cdot A_{specimen} \cdot (T_{150} - T_{151})}{m_{specimen} \cdot c_{p,specimen}} \quad (6)$$

The position of the thermocouple within the punch is represented by node 160. The temperature history at node 160 is used for comparison with the experimentally recorded temperature curve. The calculation of the time–temperature histories at each node is performed for every iteration using the differential equation solver *ode15s*. An HTC of 3.000 W/m²K was selected as the starting value for the HTC iteration. The time step size is adaptively adjusted automatically. As a result, a numerically determined temperature–time history is obtained for every node for a specific HTC value. By comparing the calculated and experimentally measured temperature histories at node 160, the coefficient of determination R^2 is calculated and passed to the optimisation module. Based on the R^2 value, the *fminsearch* function within the optimisation module determines a new HTC for the subsequent iteration. Two termination criteria were defined for the optimisation loop: a maximum of 50 iterations or an R^2 value greater than 0.98. Using the optimised HTC, the 1D FE model is solved and the calculated temperature histories are visualised. The thermophysical properties, such as thermal conductivity and specific heat capacity, were defined as temperature-dependent based on data from the JMat-Pro database. The tabular data was approximated to temperature-dependent models using polynomial functions and implemented into the 1D model. The polynomial coefficients used are listed in Table 2. This significantly reduces computational time, as there is no need to interpolate the material data as a function of the current nodal temperature at each time step for every node, but instead only evaluates the polynomial function with the respective nodal temperature.

Table 2. Coefficients of polynomial approximations for describing the thermal material data of 1.2343 and S235JR.

Material	Thermophysical property	x_3^3	x_2^2	x_1	x_0
1.2343	thermal conductivity in W/(m·K)	$9.23200 \cdot 10^{-7}$	$-3.60373 \cdot 10^{-4}$	$4.39727 \cdot 10^{-1}$	437.86345
	specific heat capacity in J/(kg·K)	$-3.50000 \cdot 10^{-8}$	$-1.55845 \cdot 10^{-5}$	$3.30995 \cdot 10^{-2}$	22.36913
S235JR	thermal conductivity in W/(m·K)	$1.03810 \cdot 10^{-6}$	$-4.14827 \cdot 10^{-4}$	$4.46068 \cdot 10^{-1}$	440.61875
	specific heat capacity in J/(kg·K)	$5.02716 \cdot 10^{-8}$	$-6.79118 \cdot 10^{-5}$	$1.20086 \cdot 10^{-7}$	47.49684

Results and Discussion

Prior to the experimental series, the influence of the cooling channels on the measured punch temperatures and the temperature evolution within the centre plate was analysed and evaluated. For this purpose, tests were carried out at a specimen temperature of 600 °C both with and without cooling, with ten repetitions approximately every 15 minutes, which represents the testing interval used in prior investigations [12]. In Fig. 3(a), the last five repetitions of the series are compared. The punch temperatures TC1, TC2 and TC3 show no deviations in the maxima. Only a time shift can be seen, as the test series with and without cooling were carried out one after the other and were not completely synchronised. The heating of the centre plate was recorded using thermocouples TC4 and TC5 positioned in front of the bearings, as shown in Fig. 3(b).

(a)

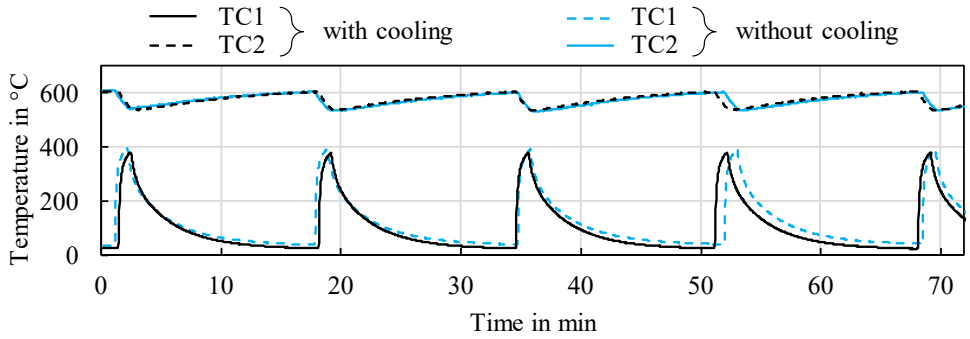

(b)

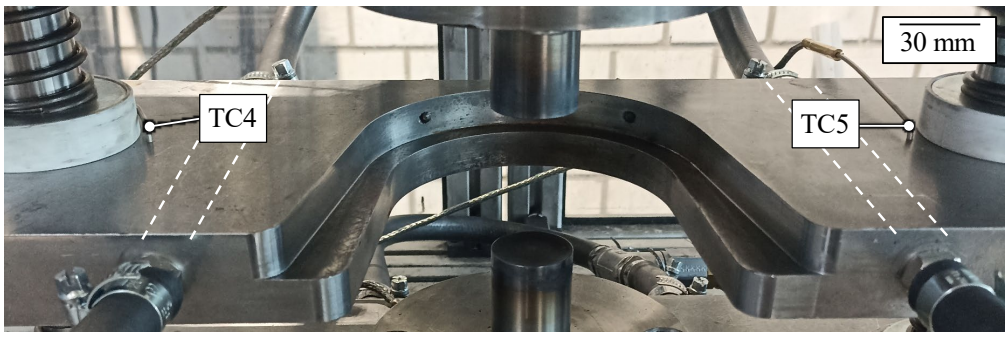

(c)

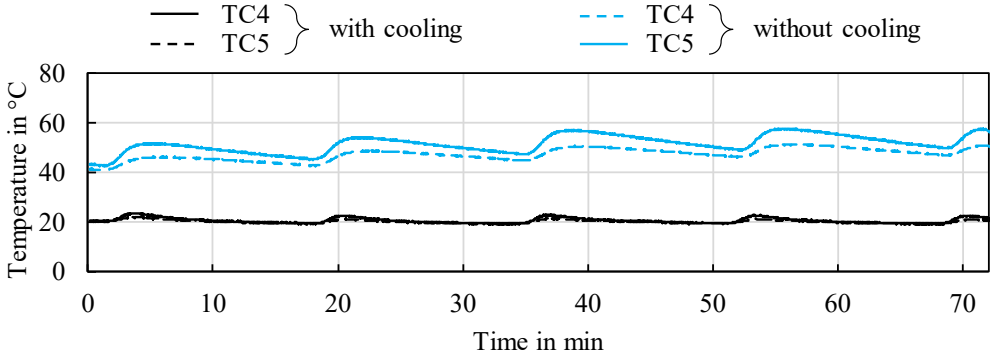

Fig. 3. (a) Temperature development for the last five repetitions of the test series with and without cooling at 600 °C for TC1 and TC2; (b) Position of thermocouples TC4 and TC5 in the middle plate; (c) Temperature development for the last five repetitions of the test series with and without cooling at 600 °C for TC4 and TC5.

In the experiment without cooling, the temperature rose by about 40 °C during the test series, while with cooling, only a partial temperature increase of about 5 °C was measured during the experiment. At a test temperature of 600 °C, this level of heating is considered non-critical. However, the use of cooling ensures constant experimental conditions. The plates are no longer subject to uncontrolled fluctuations in ambient temperature or residual heat in the plates. Instead, reproducible experimental conditions are guaranteed. Therefore, cooling was applied in all subsequent experiments.

The simulated temperature histories obtained from the 1D FE model are exemplarily shown in Fig. 4(a,b) for one experimental series conducted in an argon atmosphere without lubrication at varying contact pressures. Node 101 represents the experimentally recorded temperature measurement from thermocouple TC2 at the lateral surface of the specimen. The temperature decreases continuously from the starting temperature of 600 °C to approx. 550 °C after 50 s. The contact node 150 of the steel specimen reduces by approximately 100 °C within the first 3 s, for a contact pressure of 50 MPa, Fig. 4(a). By increasing the contact pressure to 550 MPa, the temperature at node 150 drops even more sharply within the first 3 s, by approximately 115 °C, Fig. 4(b). An even greater temperature change ΔT occurs at node 151 at the punch contact surface, amounting to approximately 225 °C. The temperature curves for node 160 and thermocouple TC1 in the experiment shown in Fig. 4(a,b) show a high degree of agreement and are almost identical, which is confirmed by the high R^2 values of 97.78% and 96.29%.

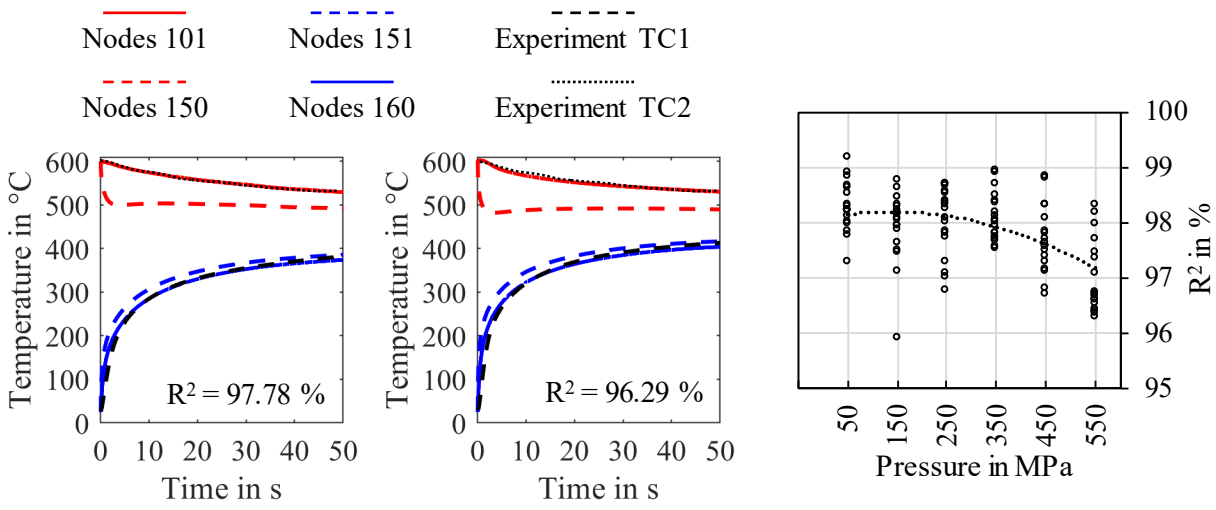

Fig. 4. Calculated temperature profiles from the 1D FE model with comparison to experimental measurements and coefficient of determination for the test series at 600 °C, argon and without lubrication under contact pressures of (a) 50 MPa; (b) 550 MPa; (c) Coefficient of determination R^2 between experimental and simulated temperature curve for experiment TC1 and node 160 via contact pressure for all tests.

Across all experiments, an R^2 value of ≥ 95 % was achieved, indicating that the experimental temperature curves are described very accurately, see Fig. 4(c). Furthermore, a general trend of decreasing R^2 values with increasing contact pressure can be observed. A possible explanation for this behaviour is the increasing plastification of the specimen, which is not taken into account in the 1D model.

The inversely and iteratively determined HTCs for the investigated parameter configurations are plotted as a function of the contact pressure in Fig. 5. In addition to the three repetitions of each parameter combination, the average HTC value of the three data points was calculated and is shown as a line. For the test series conducted under argon, shown in Fig. 5(a–c), all results exhibit a linear trend, independent of the lubrication condition, describing a continuous increase in the HTC with rising contact pressure. An increasing HTC with increasing contact pressure was also observed in the work of Wen et al. for 22MnB5 sheet metal up to a maximum contact pressure of 50 MPa [6].

One possible explanation is that, with rising contact pressure, the surface asperities of the softer contact partner are progressively flattened, thereby increasing the real contact area available for heat transfer. The individual data points are located very close to the mean curve, indicating a high reproducibility of the experiments.

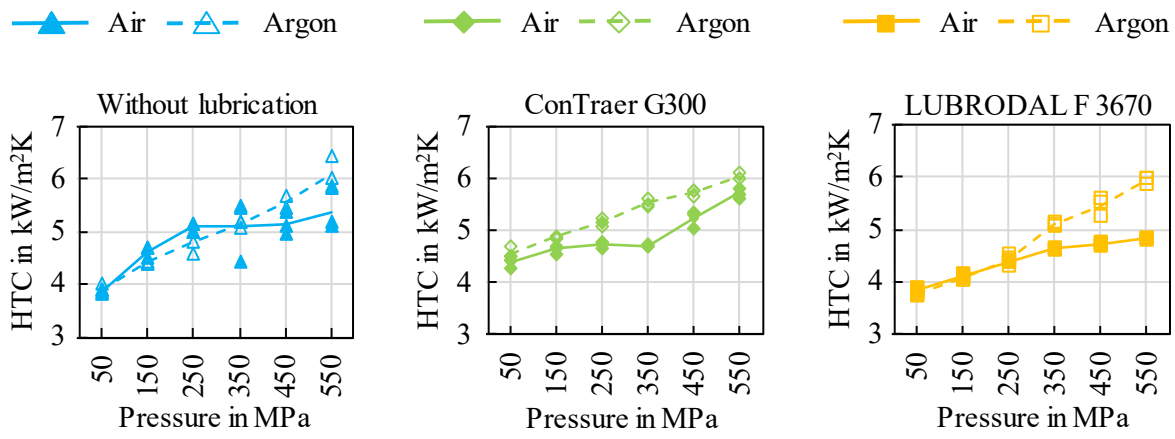

(a) (b) (c)

Fig. 5. Development and comparison of pressure-dependent HTC between air and argon (a) without lubrication; (b) ConTraer G300; (c) LUBRODAL F 3670.

The test series carried out in air initially also show a linear increase in HTC with rising contact pressure. At a contact pressure of 250 MPa, the HTC stagnates for the tests without lubrication, Fig. 5(a) and with ConTraer G300, Fig. 5(b). A possible explanation is that, with the onset of plastification, the oxide- and lubricant-covered surface locally ruptures. This reduces the real contact area, so that the HTC no longer increases despite rising contact pressure. Only with a further increase in contact pressure are the ruptured surfaces closed again, causing the HTC to increase once more. In the case of LUBRODAL F 3670, no stagnation is observed in the range between 250 and 350 MPa, see Fig. 5(c). Instead, the slope of the linear increase merely flattens at a contact pressure of 350 MPa. Although the oil-based lubricant evaporates at the applied temperature of 600 °C, it cannot be ruled out that the remaining lubricant layer exhibits higher elasticity compared to ConTraer G300. As a result, the lubricant film may remain intact despite local surface rupture, thus continuing to impede heat transfer. The fact that, regardless of the selected atmosphere, a lower HTC is determined for LUBRODAL F 3670 compared to ConTraer G300 indicates that LUBRODAL F 3670 reduces heat transport even after evaporation of the carrier medium. That LUBRODAL F 3670 exhibits a reduced HTC when the carrier medium is no longer present in the contact zone was also clearly demonstrated in a previous work of the authors during the determination of the HTC for an EN AW-6082 / 1.2343 contact. At 300 °C and contact pressures of up to 200 MPa, a higher HTC was achieved with LUBRODAL F 3670 than with ConTraer G300, which was attributed to the improved wetting of the contact surface by the oil-based carrier medium. At higher contact pressures, however, the HTC decreased rapidly to values below those obtained with ConTraer G300. Due to the increasing pressure, the carrier medium was expelled from the contact zone, leaving only the solid lubricant particles in contact, which reduced heat transport [12]. At 600 °C, the carrier medium evaporates immediately after contact, so that only solid lubricant particles remain in the contact zone.

The influence of oxides in the contact zone is evident from the direct comparison of the HTC curves obtained in air and under argon for all lubrication conditions in Fig. 5(a-c). The HTCs determined under argon are generally higher than the HTC of oxide covered, particularly at contact pressures above 350 MPa. This difference may be attributed to the onset of plastification, since the increase in surface area causes the oxide layers to fracture, thereby reducing the real contact area. At contact pressures below 250 MPa, the specimens are loaded only elastically, so that no increase in surface area occurs and the contact area remains comparable. With the exception of the tests at contact

pressures below 350 MPa without lubrication, the oxide layer in the contact zone generally slows down heat transport, resulting in a reduced HTC.

The formed oxide scale was measured using a confocal microscope, yielding an oxide layer thickness of approximately 80 µm. The scaled specimen is shown in Fig. 6(a). With an increase in application temperature to 900 °C, enhanced oxide formation is to be expected. Bergelt et al. showed in their studies that after only 2 min at 900 °C, an oxide scale thickness of approximately 40 µm had already formed [15]. Due to the slow heating in the chamber furnace of approximately 30–40 min, substantial scale formation must be expected, making investigations with and without argon atmosphere indispensable for studies at higher temperatures.

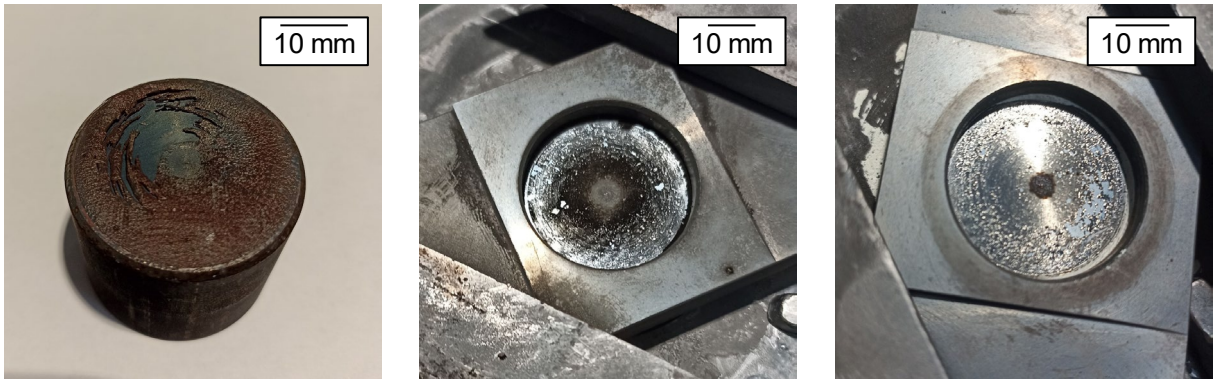

(a) (b) (c)

Fig. 6. (a) Cooled and extracted specimens after testing at 600 °C under air without lubrication and 50 MPa with scale formation; end face of the specimen directly after testing at 600 °C, without lubrication, 50 MPa (b) under air and (c) under argon atmosphere.

In Fig. 6(b,c), the underside of the specimen holder after a test at 50 MPa without lubrication is shown, revealing the end face of the specimen. The specimen in Fig. 6(b) was heated in air, whereas the specimen in Fig. 6(c) was heated under protective gas. It can be observed that even the specimen heated under protective gas exhibits slight oxide formation. This indicates that continuous scale formation already occurs during the transfer from the furnace to the test rig and during the time until the punches come into contact with the specimen surface. This scale formation represents a limitation of the experimental setup and must be taken into account in the interpretation of the results and in further investigations.

Summary and Conclusion

Compound forging offers considerable potential for lightweight design through the integration of dissimilar materials within a single forming operation. However, the numerical design of such processes is strongly dependent on an accurate description of thermal boundary conditions, in particular the HTC at the workpiece–die interface. Due to the lack of experimentally validated data under forging-relevant conditions, the HTC is frequently assumed to be constant in numerical simulations, which limits their predictive capability.

In this study, a dedicated experimental–numerical methodology was developed to determine load-dependent HTCs representative of hot bulk and compound forging processes. A specialised test rig enabled the reproduction of high contact pressures, including pressure levels exceeding the flow stress of the workpiece, while maintaining controlled thermal conditions. Temperature histories were measured close to the contact interface using embedded thermocouples and evaluated by means of an inverse optimisation approach based on a one-dimensional finite element model. This approach allowed the HTC to be iteratively identified by matching simulated and experimental temperature evolutions with high coefficients of determination.

The results demonstrate a clear dependence of the HTC on contact pressure across all investigated conditions. Under a protective argon atmosphere, the HTC increased almost linearly with rising pressure, largely independent of lubrication, indicating an increasing real contact area as surface

asperities were progressively flattened. In contrast, experiments conducted in air revealed deviations from this linear trend at intermediate pressure levels, which were attributed to oxide scale formation and local surface rupture during the onset of plastic deformation. Lubrication was shown to reduce heat transfer in all cases, with oil-based lubricants exhibiting a pronounced insulating effect due to residual solid lubricant particles remaining in the contact zone at elevated temperatures.
Overall, the findings confirm that the HTC in compound forging cannot be represented by a constant value but must instead be described as a function of contact pressure, atmosphere, and lubrication condition. The HTC data generated in this work provides a robust basis for improving the accuracy of finite element simulations of compound forging processes. Their implementation enables more reliable prediction of temperature fields, material flow behaviour, and interfacial phenomena, thereby supporting robust process design and facilitating the industrial application of hybrid forged components.
In future work, experiments will be conducted at temperatures of up to 900 °C in order to determine the HTC for steel under forging-relevant thermal conditions. In addition, controlled heating of the punches by means of heating sleeves will be integrated to further adapt the experimental setup to the boundary conditions of hot bulk forming. To enable the application of the determined heat transfer coefficients in finite element simulations, the obtained findings will be transferred into a model for the mathematical description of the variable-dependent heat transfer coefficient. This will allow heat transfer to be considered as a spatially and temporally dependent quantity in process simulations, thereby not only improving the prediction of the thermal workpiece history but also enabling targeted measures for process control and optimisation.

Acknowledgment

Funded by the Deutsche Forschungsgemeinschaft (DFG, German Research Foundation) – Projektnummer (496068488).

References

[1] J. Shen, Q. Zhang, S. Tian, Impact of the vehicle lightweighting and electrification on the trend of carbon emissions from automotive materials, J. Clean. Prod. 513 (2025) 145677. https://doi.org/10.1016/j.jclepro.2025.145677.

[2] O. Music, J.M. Allwood, Connecting environmental systems analysis to manufacturing technology: A catalogue of the world's steel and aluminium components, Resour. Conserv. Recycl. 212 (2025) 107949. https://doi.org/10.1016/j.resconrec.2024.107949.

[3] B.-A. Behrens, K.-G. Kosch, C. Frischkorn, N. Vahed, A. Huskic, Compound forging of hybrid powder-solid-parts made of steel and aluminum, Key Eng. Mater. 504–506 (2012) 175–180. https://doi.org/10.4028/www.scientific.net/KEM.504-506.175.

[4] B.-A. Behrens, J. Uhe, T. Petersen, C. Klose, S.E. Thürer, J. Diefenbach, A. Chugreeva, Challenges in the Forging of Steel-Aluminum Bearing Bushings, Materials 14 (4) (2021) 803. https://doi.org/10.3390/ma14040803.

[5] G. Veiga-Piñeiro, E. Martín-Ortega, S. Pérez-Betanzos, Thermal Management in Multi-Stage Hot Forging: Computational Advances in Contact and Spray-Cooling Modelling, Materials 18 (14) (2025) 3318. https://doi.org/10.3390/ma18143318.

[6] S. Wen, Z. Chen, S. Qu, J.J. Tang, X. Han, Investigations on the interfacial heat transfer coefficient during hot stamping of ultra-high strength steel with Al-Si coating, Int. J. Heat Mass Transf. 189 (2022) 122739. https://doi.org/10.1016/j.ijheatmasstransfer.2022.122739.

[7] B.-A. Behrens, C. Klose, A. Chugreev, N. Heimes, S.E. Thürer, J. Uhe, A Numerical Study on Co-Extrusion to Produce Coaxial Aluminum-Steel Compounds with Longitudinal Weld Seams, Metals 8 (2018) 717. https://doi.org/10.3390/met8090717.

[8] A.R. Singh, A.S. Bhattacharya, C. Butcher, K.J. Daun, Experimental artefacts affecting characterization of the evolving interfacial heat transfer coefficient in hot stamping of Al-Si coated 22MnB5 steel, Appl. Therm. Eng. 236 (Part B) (2024) 121604. https://doi.org/10.1016/j.applthermaleng.2023.121604.

[9] S. Dixit, T. Altan, D.R. Mahapatra, Determination of temperature distribution in cold forging with the support of inverse analysis, Measurement 187 (2022) 110270. https://doi.org/10.1016/j.measurement.2021.110270.

[10] P. Volke, P. Groche, Interfacial heat transfer coefficients in cold forging of stainless steel, Int. J. Mater. Form. 15 (2022) 32. https://doi.org/10.1007/s12289-022-01688-2.

[11] A.S. Bhattacharya, K.N. Adhvaryu, A.R. Singh, C. Butcher, K.J. Daun, Influence of the coating on the interfacial heat transfer coefficient in hot stamping of Al-Si coated 22MnB5 steel, Int. J. Adv. Manuf. Technol. 137 (2025) 3049–3059. https://doi.org/10.1007/s00170-025-15339-8.

[12] N. Mohnfeld, H. Wester, R. Grawe, S. Peddinghaus, J. Uhe, B.-A. Behrens, Experimentell-Numerische Ermittlung des Wärmeübergangskoeffizienten für EN AW-6082: Wärmeübergangskoeffizienten für die Warmmassivumformung, WT Werkstattstechnik 115 (2025) 741–749. https://doi.org/10.37544/1436-4980-2025-10-45.

[13] B.-A. Behrens, J. Uhe, H. Wester, N. Mohnfeld, Development of a test setup for the experimental determination of the heat transfer coefficient for compound forging, in: Proceedings 33rd International Conference on Metallurgy and Materials (METAL 2024), Brno, Czech Republic, 2024, pp. 75–80. https://doi.org/10.37904/metal.2024.4871.

[14] M. Pietsch, M. Mennig, Pad Printing, in: M.A. Aegerter, M. Mennig (Eds.), Sol-Gel Technologies for Glass Producers and Users, Springer, Boston, MA, 2004, pp. 123–125. https://doi.org/10.1007/978-0-387-88953-5_15.

[15] T. Bergelt, M. Graf, J. Hunze-Tretow, B.-A. Behrens, T. Lampke, Modelling of dynamic scale layer growth considering temperature, time and alloying elements, Mater. Res. Proc. 44 (2024) 482–492. https://doi.org/10.21741/9781644903254-52.

The publication of this article was funded by the Leibniz Universität Hannover (LUH) / Technische Informationsbibliothek (TIB)